ACS APPLIED MATERIALS & INTERFACES

Research Article

www.acsami.org

Hybrid Perovskite Quantum Nanostructures Synthesized by Electrospray Antisolvent–Solvent Extraction and Intercalation

Rounak Naphade,[*,†,‡] Satyawan Nagane,[†,‡] G. Shiva Shanker,[§] Rohan Fernandes,[∥] Dushyant Kothari,[∥] Yuanyuan Zhou,[⊥] Nitin P. Padture,[⊥] and Satishchandra Ogale[*,†,§]

[†]Centre of Excellence in Solar Energy, Physical and Material Chemistry Division, National Chemical Laboratory (NCL) Pune, 411 008, India

[‡]Academy of Scientific and Innovative Research (AcSIR), Anusandhan Bhawan, 2 Rafi Marg, New Delhi 110 001, India

[§]Department of Physics and Centre for Energy Science, Indian Institute of Science Education and Research (IISER), Dr. Homi Bhabha Road, Pune 411 008, India

[∥]Department of Physics and National Centre for Nanosciences & Nanotechnology, University of Mumbai, Vidyanagari, Santacruz (E), Mumbai 400 098, India

[⊥]School of Engineering, Brown University, Providence, Rhode Island 02912, United States

Supporting Information

ABSTRACT: Perovskites based on organometal lead halides have attracted great deal of scientific attention recently in the context of solar cells and optoelectronic devices due to their unique and tunable electronic and optical properties. Herein, we show that the use of electrospray technique in conjunction with the antisolvent–solvent extraction leads to novel low-dimensional quantum structures (especially 2-D nanosheets) of $CH_3NH_3PbI_3$- and $CH_3NH_3PbBr_3$-based layered perovskites with unusual luminescence properties. We also show that the optical bandgaps and emission characteristics of these colloidal nanomaterials can be tuned over a broad range of visible spectral region by compositional tailoring of mixed-halide (I- and Br-based) perovskites.

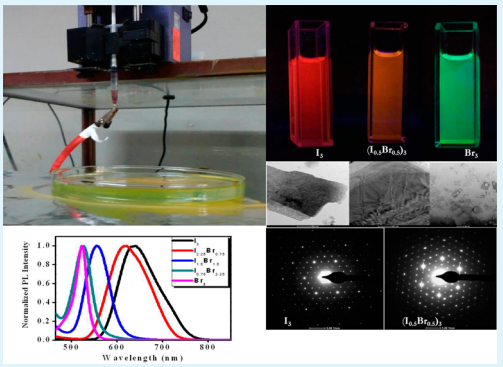

KEYWORDS: *perovskite, 2D nanostructure systems, quantum dots, nanosheets, antisolvent–solvent extraction, electrospray, bandgap tuning*

1. INTRODUCTION

Organometal–halide perovskites have been receiving significant attention recently due to their distinctive electronic and optical properties, which have led to record high power conversion efficiency (PCE) of >20% in solution-processed perovskite solar cells (PSCs).[1−5] These properties include strong broad-band absorption, tunable optical properties, and the ambipolar nature of charge carriers with long lifetimes, which are under intense scientific investigations at this time. The 3-D perovskite structure, with a general formula of ABX_3, is versatile and allows substitutions of a variety of organic cations (A), divalent metal ions (B), and halogens (X), resulting in tunable changes in their optical and electronic properties. More recently, researchers have been developing synthesis approaches to create a variety of nanostructures of organolead-halide hybrid perovskites to expand the property space and to achieve altogether new properties through quantum effects.[6,7] These nanostructures possess high quantum yield and strong optically tunable fluorescence with narrow emission bandwidths, making them suitable for diode and lasing applications.[8] Some research groups have used antisolvent crystallization approach[9−11] to obtain 0-D (quantum dots or QDs), 1-D (nanorods, nanobelts, nanowires), 2-D (nanosheets) $CH_3NH_3PbX_3$ ($MAPbX_3$)-based perovskites. This antisolvent crystallization approach has also been used to obtain films of 3-D hybrid perovskite (without any organic moiety for intercalation) and shown to improve the photovoltaic performance of hybrid solar cells.[12]

Recently, Zhou et al.[13] demonstrated a room-temperature antisolvent–solvent extraction (ASE) process for the synthesis of dense, ultrasmooth $MAPbI_3$ perovskite thin films. In that approach, the $MAPbI_3$ precursor solution in *N*-methyl-2-pyrollidone (NMP) solvent was spin-coated on a substrate, and then the wet film was immediately dipped in a bath of a second solvent, diethyl ether (DEE), to facilitate rapid nucleation and growth of perovskite crystals. Planar PSCs fabricated from those films delivered up to 15% PCE.

In this work, we build upon this simple, scalable antisolvent–solvent extraction (ASE) approach for the synthesis of unusual,

Received: October 25, 2015
Accepted: December 21, 2015
Published: December 21, 2015

DOI: 10.1021/acsami.5b10208
ACS Appl. Mater. Interfaces 2016, 8, 854–861

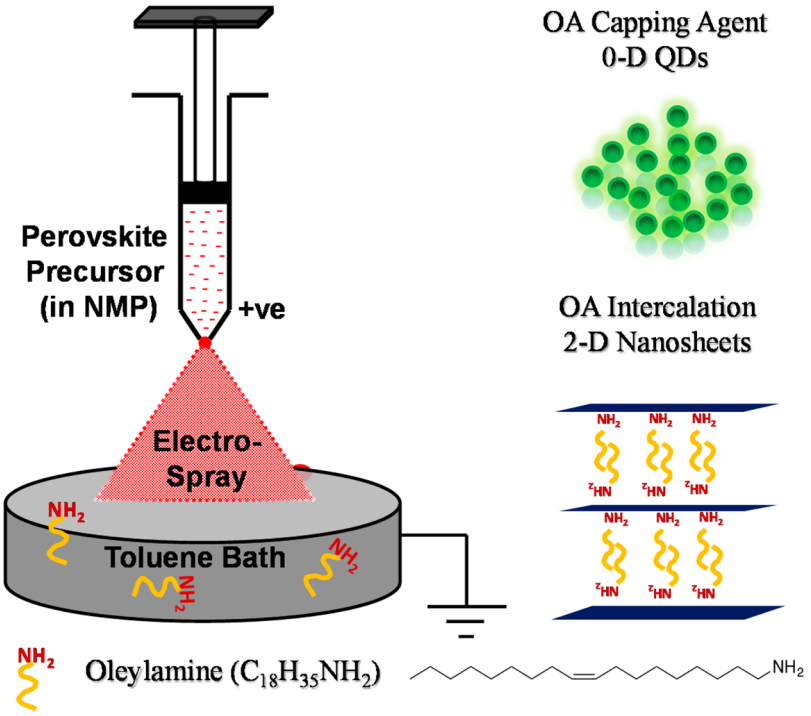

Figure 1. Schematic illustration of the synthesis of $MAPbX_3$ perovskite quantum structures by electrospray antisolvent−solvent extraction (ASE) route.

low-dimensional $MAPbX_3$-based perovskite colloidal nanostructures in a single step. This is accomplished by combining the ASE technique with the electrospray process. Electrospray is a versatile method for materials growth[14] in which fine liquid droplets are dispensed from a sharp tip onto a metal or a metal−supported substrate under an applied electric field between the tip and the substrate. In this method, no polymers (or macromolecules) are used; instead, only fine liquid droplets are dispensed.

In the present work, we use a novel variant of the commonly used electrospinning or electrospray method, where instead of a solid substrate a bath of the antisolvent (without and with a capping agent) in a metal-electrode container is used as the substrate. A schematic illustration of this process is shown in Figure 1. In this process, under the high electric field the surface tension of a droplet breaks it into a jet of nanodroplets of the precursor solution which fall into antisolvent (toluene) bath, resulting in rapid crystallization of the perovskite leading to uncapped 0-D nanoparticles. In related experiments, we have also used oleylamine (OA) as a capping agent in the toluene bath to arrest the nanoparticle growth. OA ($C_{18}H_{35}NH_2$) is a long-chain neutral alkyl molecule with amine ($-NH_2$) functionality, which not only serves as a capping agent but, more interestingly, also contributes to the formation of 2-D sheet-like quantum structures of layered perovskites by intercalation via host−guest chemistry. This leads to anisotropic quantum confinement of excitons which influences their luminescence properties.

Recently, it has been shown that mixed-halide-based perovskites hold great promise for applications in the area of laser diodes and light emitting diodes (LEDs).[15] The mixed-halide perovskite compositions offer advantages of bandgap tuning over a wide visible spectrum.[16] Thus, we have also synthesized mixed-halide perovskite ($MAPbI_{(3-x)}Br_x$) nanostructures using this method by simply mixing the $MAPbI_3$ and $MAPbBr_3$ precursor solutions in different proportions. We show that the optical bandgaps and photoluminescence (PL) of these colloidal solutions can be tuned over a wide wavelength range of 500−700 nm.

2. EXPERIMENTAL PROCEDURE

2.1. Materials. All chemicals and solvents were used as-received without further purification, and included PbI_2 (lead iodide 99% pure, Alfa Aesar), $PbBr_2$ (lead bromide. 99% pure, Alfa Aesar), hydroiodic acid (HI; 57 wt % in water, Sigma-Aldrich), hydrobromic acid (HBr; 48 wt % in water, Sigma-Aldrich), methylamine (CH_3NH_2; 33 wt % solution in absolute ethanol, Sigma-Aldrich), oleylamine (OA; Sigma-Aldrich), *N*-methyl-2-pyroliddone (NMP; Analytical grade Chem Laboratories), and toluene (Analytical grade Chem Laboratories).

2.2. Synthesis of $MAPbX_3$ Nanomaterials. For $MAPbI_3$, 1 mM of PbI_2 and 1 mM of MAI were dissolved in 2 mL of NMP for about 6 h. After we ensured the homogeneity of the solution, it was fed into the 1 mL DISPO VAN syringe (26 gauge). This solution was dispensed at a flow rate of 0.6 mL/h under a very high electric field of 1.8 kV/cm. The distance between the needle and collector was kept at 10 cm. The jet of droplets thus formed were directed into an antisolvent bath of liquid held in a metal container used as the ground terminal. This bath contained either toluene or toluene with the OA capping agent dissolved in it. The $MAPbBr_3$-based nanostructures were also fabricated using the same strategy with 1 mM of $PbBr_2$ and 1 mM of MABr as the precursors. The amount of OA in toluene was varied systematically to prepare $MAPbI_3$ QDs. For the synthesis of mixed-halide-based layered perovskites separate precursor solutions of $MAPbI_3$ and $MAPbBr_3$ were mixed in 1:3, 1:1, and 3:1 ratios. The experimental conditions for these electrospraying experiments were the same as above. In additional experiments, the $MAPbI_3$ precursor was directly electrosprayed into 100 mL of toluene bath without OA for about 20 min, followed by the quick addition of 100 μL of OA to the toluene bath.

2.3. Characterization. X-ray diffraction (XRD) patterns were recorded using a powder diffractometer (Xpert 1712, PANanalytical) using monochromatic Cu Kα X-ray radiation (λ = 1.5402 Å). An ultraviolet−visible (UV−vis) spectrophotometer (LAMBDA 950, PerkinElmer) was used to collect the absorption spectra. PL spectra (Fluoromax 4C, Horiba) and PL lifetime (FLS980, Edinburgh Instruments) measurements were also performed on the nanostructures produced. Surface properties of the nanostructures were characterized

DOI: 10.1021/acsami.5b10208
ACS Appl. Mater. Interfaces 2016, 8, 854−861

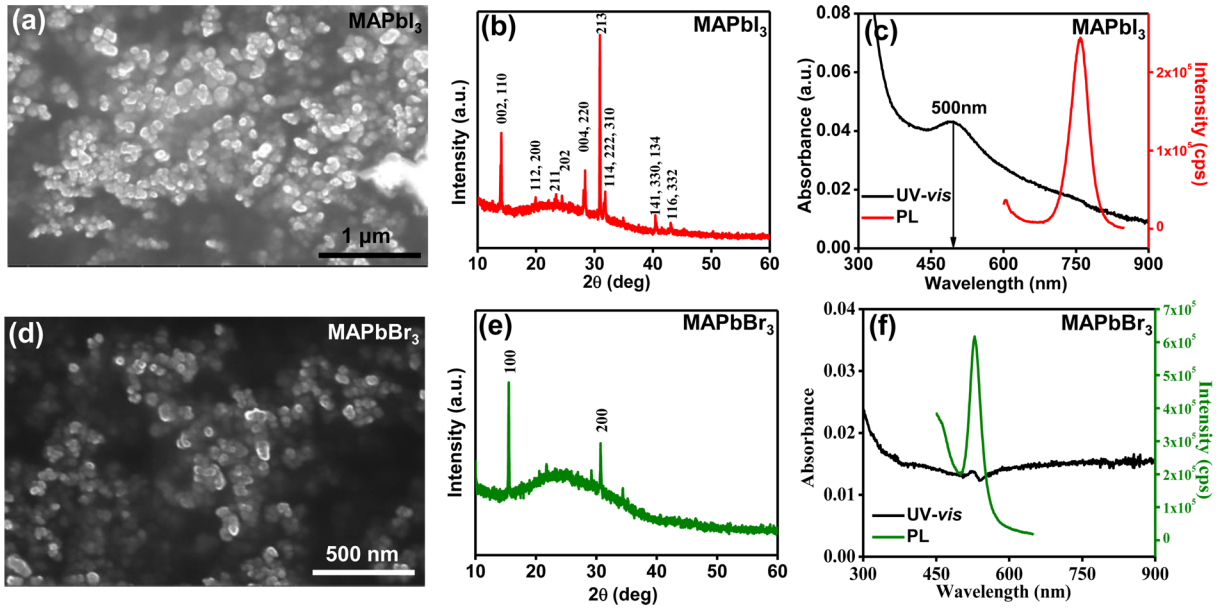

Figure 2. SEM images of the nanoparticles: (a) $MAPbI_3$ and (d) $MAPbBr_3$. Indexed XRD patterns of the nanoparticles: (b) $MAPbI_3$ and (e) $MAPbBr_3$. UV−vis and PL spectra (excitation wavelength 510 nm for $MAPbI_3$ and 400 nm for $MAPbBr_3$) of the nanoparticles: (c) $MAPbI_3$ and (f) $MAPbBr_3$.

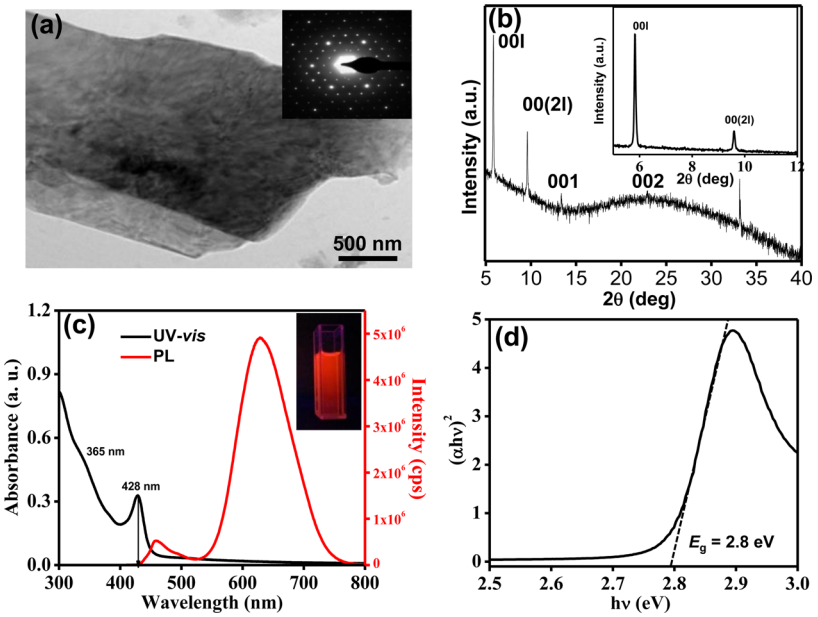

Figure 3. $MAPbI_3$-based layered 2-D perovskite nanostructures: (a) TEM image and (inset) selected-area electron diffraction pattern, (b) XRD pattern, (c) UV−vis and PL spectra (excitation wavelength 365 nm) and (inset) photograph of the colloid, and (d) Tauc plot obtained from the UV−vis data.

using X-ray photoelectron spectroscopy (XPS; Phi 5000 VersaProbe II, Physical Electronics, ULVAC PHI) equipped with a monochromatic Al Kα (λ = 1486.6 eV) X-ray radiation and a hemispherical analyzer. The atomic force microscopy (AFM) imaging and height profile measurements on exfoliated sheets were performed using a Nanosurf Atomic Force Microscope. Here, the specimens were prepared in a glovebox and hermetically sealed. Just before the XPS characterization, the specimens were opened and immediately loaded into the XPS chamber to avoid any ambient degradation. For recording the XRD, AFM, and XPS data, the specimens were prepared by drop-casting the colloidal dispersion in toluene on a Si wafer and drying. In the case of transmission electron microscopy (TEM) characterization (300 T-30 Tecnai, FEI Corp.), the colloidal dispersion in toluene was drop-cast on carbon-coated TEM copper grids and dried.

3. RESULTS AND DISCUSSION

3.1. $MAPbI_3$ and $MAPbBr_3$ 3-D Perovskites Grown without Oleylamine. Initially, the $MAPbI_3$ precursor solution was electrosprayed directly into the toluene bath which contained no capping agent. This resulted in the formation of nanoparticles of average size 50 ± 15 nm (Figure 2a,d). The indexed XRD pattern in Figure 2b confirms the tetragonal phase of $MAPbI_3$ (space group $I4/mcm$). The UV−vis spectrum in Figure 2c shows a broad absorption feature over the entire visible range.

Similarly, the PL spectrum shows broad fluorescence centered at ∼760 nm. This is blue-shifted by ∼20 nm as compared to the bulk perovskite case.[17] In the case of $MAPbBr_3$ (Figure 2d,e) the

DOI: 10.1021/acsami.5b10208
ACS Appl. Mater. Interfaces 2016, 8, 854−861

nanoparticles (~50 nm) are of cubic phase (space group $Pm\bar{3}m$), with a narrower PL peak centered around 550 nm.

It has been reported that long alkyl-chain-based ammonium salts can be used to create different types of perovskite nanostructures.[9] Here, we have used OA as a neutral ligand[18] in the antisolvent toluene bath to serve a dual purpose, namely capping agent and intercalation agent, for the spray of the perovskite precursors falling into the bath. Note that other long alkyl-chain-based ammonium salts, such as *n*-octylammoium bromide and *n*-butylammonium bromide salts,[19−21] can also be used in this method.

Initially, experiments were performed using OA quantity varying over the range of 50−100 μL in a 100 mL toluene bath to determine the effect of OA concentration on the nature of quantum structures formed. Figure S1 (Supporting Information) shows the FE-SEM images for three such cases. With 50 μL of OA we observed the assembly of nanoparticles, along with sheet-like structures. As the amount of OA was increased to 80 μL, the sheet-like structures were found to increase. However, some nanoparticles-assembly was still seen to be present in that sample. For the case of 100 μL OA only sheet-like structures were observed. We also measured Photoluminescence (PL) spectra of the colloidal solutions obtained for the cases of different OA concentrations. A strong blue shift in the PL-peak maximum, with additional shoulder between 700 and 730 nm is observed for 50 μL and 80 μL OA amounts. Zhang et al.[10] have reported similar PL peak at 734 nm for $MAPbI_3$ quantum dots. However, the shoulder disappears as the amount of OA is increased to 100 μL in the toluene bath, with the PL-peak maximum occurring at 630 nm (Figure S2 Supporting Information). This large blue-shift of ~130 nm suggests that the OA is not only acting as a capping agent but it also plays a role in modifying the perovskite crystal structure itself. Thus, all further experiments used 100 μL of OA in 100 mL of toluene bath.

3.2. $MAPbI_3$-based Layered 2-D Perovskites Grown with Oleylamine. The TEM image in Figure 3a shows nanosheet-like 2-D layered perovskite. The areal sizes of these nanosheets are quite large, in the micron range. Additionally, the "spot" selected-area electron diffraction pattern (SAEDP) in the inset of Figure 3a confirms the single-crystal nature of the 2-D perovskite nanosheets. The structure of this 2-D perovskite comprises ordered hexagonal arrangement of PbI_2 octahedrons in a sheet, with these sheets stacked together through the organic ligand.[22,23]

As mentioned earlier, when the $MAPbI_3$ precursor solution falls into toluene bath it crystallizes immediately leading to the perovskite formation. The presence of OA in the same bath can act as a guest molecule, and it can intercalate between the thin layers of PbI_2. This OA intercalation results in distortion of PbI_6^{4-} octahedra, and hence the as-formed perovskite is stabilized in the 2D perovskite structure.

The OA intercalation can be further confirmed by the XRD results in Figure 3b where high intensity peaks at very low values of 2θ = 5.8° and 2θ = 9.6° are observed. This implies high interplanar spacing, corresponding to 00l and 00($2l$) reflections, respectively, where l = 2, 4, 6..., for layered perovskite with monoclinic symmetry.[24] The interlayer spacings (d_{00l}) for 2θ = 5.8° and ($d_{00(2l)}$) for 2θ = 9.6° are 15.22 and 9.21 Å, respectively. The crystal orientation of this 2-D perovskite suggests periodic arrangement of inorganic layers comprised of PbI_2 sheets formed by series of PbI_6^{4-} based octahedra and OA-based organic ligands intercalated in between, oriented along the *c*-axis. In addition to sharp peaks at low 2θ, a hump at 2θ in the 20−30° range is also observed, which can be attributed to broadened (002) reflections from the PbI_2 nanosheets. Thus, the TEM and XRD results confirm the formation of highly oriented single-crystalline intercalated layered 2-D perovskite along with the formation of PbI_2 nanosheets comprising PbI_6^{4-}octahedrons. Note that Mitzi and co-workers[25] had shown occurrence of a series of such Sn-based layered 2-D perovskite phases at low temperatures.

Further, we performed the AFM analysis to quantify the minimum thickness of 2-D sheets when the corresponding dilute solution is drop casted onto a silicon wafer surface. As may be seen from Figure S3 (Supporting Information) the minimum thickness is about 3−4 nm. At some places, the sheets have clearly stacked up enhancing the height, as expected. The lateral width of the thinnest sheets is of the order of 400−500 nm.

The UV−vis data in Figure 3c shows strong absorption edge at λ = 428 nm, which has a large blue-shift as compared with bulk $MAPbI_3$.[26] In addition, a broad absorption peak around ~365 nm is observed in the UV region, which also confirms the presence of nanosized PbI_2 quantum dots.[27] It has been reported that because the inorganic framework is separated by organic molecule intercalation in layered 2-D perovskites, such systems show high oscillator strength at room temperature due to large dielectric mismatch, resulting in naturally formed quantum well structures with stable exciton binding energies.[28] From the Tauc plot (Figure 3d), the band gap of this layered perovskite was found to be 2.8 eV, which is much higher than that of the bulk $MAPbI_3$ perovskite (1.55 eV). This significant increase in the band gap can be attributed to strong anisotropic quantum confinement effects arising from the naturally formed quantum well structures. The PL spectrum in Figure 3c also shows a broad emission centered at ~630 nm with a full-width half-maximum (fwhm) of ~102 nm, in addition to a very large Stokes shift.

Recently Wu et al.[29] have hypothesized that the formation of "self-trapped exciton" is facilitated by going from 3-D perovskite to 2-D perovskites, and the corresponding density increases. Self-trapped exciton can be ascribed to the formation of excited state as a result of the highly covalent nature of lead-iodide backbone. Ahmad et al.[30] have also discussed the formation of self-trapped exciton in the case of lead-halide-based layered structures formed by using long alkyl-chained amines as intercalating agents. Another cause for large Stokes shift may be stacking of a few 2-D sheets leading to the formation of stable low energy band states contributing to the exciton emission.[29] A large Stokes shift is also reported very recently in the case of hybrid-perovskite QDs.[10]

Because crystallization of the perovskite phase and intercalation of OA in-between the PbI_2 layers are kinetically competing processes in the bath, to gain deeper insight into the OA intercalation process, OA was added to the antisolvent bath after perovskite crystallization. The UV−vis spectrum for those samples shown in Figure 4 reveals multiple absorptions at 365, 510, and 571 nm. The peaks at 510 and 571 nm are due to the 3-D $MAPbI_3$ perovskite, and the peak at 365 nm is due to nanosized PbI_2 particles. These results suggest that the OA addition after electrospray affects the as-formed perovskite nanoparticles by decomposing them into PbI_2 QD, and that only the presence of OA in the toluene bath during electrospray results in its intercalation leading to formation of layered 2-D perovskite.

The PL decay dynamics for the case of $MAPbI_3$-based layered 2-D perovskite is shown in Figure 5. The PL decay was fitted with biexponential decay resulting in lifetimes of τ_1 = 20 ns (35.5%) and τ_2 = 74 ns (64.5%). Such biexponential decay confirms the presence of two different species involved in the recombination

DOI: 10.1021/acsami.5b10208
ACS Appl. Mater. Interfaces 2016, 8, 854−861

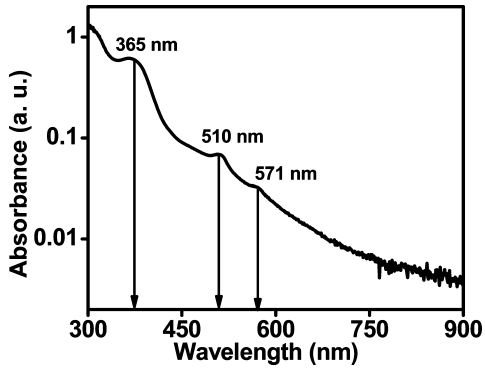

Figure 4. UV−vis spectrum of $MAPbI_3$-based nanostructures formed in Toluene bath where the OA is added after the crystallization is complete.

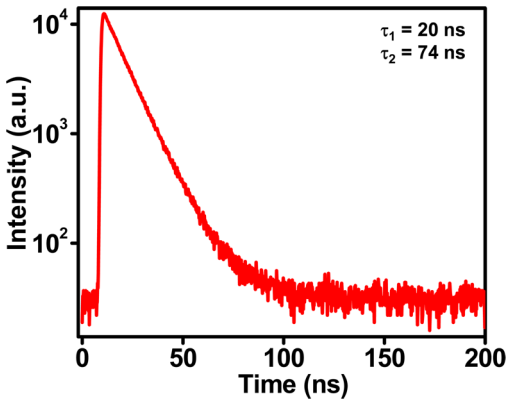

Figure 5. PL (excitation wavelength 400 nm) lifetime decay for $MAPbI_3$-based layered 2-D perovskite nanostructures (biexponential fit).

process. The relatively long lifetimes confirm the presence of surface trap states produced by the isolated PbI_2-based octahedra.[31] Such defect centers are mainly responsible for the large Stokes shift and the longer lifetime decays.

3.3. $MAPbBr_3$−Based Layered 2-D Perovskites Grown with Oleylamine. The TEM images in Figure 6a,b show the presence of 2-D nanosheets and 0-D QDs, respectively, of the $MAPbBr_3$-based perovskite. The size of the monodispersed quantum dots (Figure 6b) is ∼2−3 nm. The XRD pattern in Figure 6c shows the corresponding peak broadening, and sharp peaks at small 2θ (5°−10°) similar to what is observed in Figure 3b. The PL spectrum in Figure 6d shows a single emission centered at ∼520 nm.

The strong quantum confinement effect is primarily responsible for the observed blue-shift vis-a-vis the bulk 3-D perovskite.[32] This sharp PL emission is mainly an excitonic emission with a narrow line width of ∼25 nm. It should be noted that the Pb−I bond is more polar than the Pb−Br bond, hence the precursor droplets falling in the bath are stabilized more rapidly in the Pb−Br case leading to higher density of capped QDs.[33−35]

Thus, in the bromine-based perovskite case, the role of OA as capping agent is more effective in stabilizing the 0-D QD, although some 2-D sheets are also seen due to its role as the intercalating organic moiety. The Tauc plot in Figure 6e shows two distinctive band gaps of E_g = 2.2 eV for QDs and E_g = 2.9 eV for the layered 2-D perovskite.

The PL decay dynamics for $MAPbBr_3$-based colloidal solution was also studied for recombination lifetimes (Figure 6c). The PL decay is fitted using a triexponential function, with lifetimes τ_1 = 5.7 ns (40.4%), τ_2 = 16.2 ns (41.5%), and long-lived carriers with τ_3 = 125 ns (18.1%). The relative contribution of long-lived carriers is significantly less as compared to the earlier reported work.[10]

3.4. $MAPbI_{(3-x)}Br_x$ Mixed-Halide Layered 2-D Perovskites Grown with Oleylamine. The TEM image of mixed-halide $MAPbI_{1.5}Br_{1.5}$-based layered 2-D perovskite in Figure 7a shows a nanosheet (wrinkled), and the "spot" SAEDP (inset)

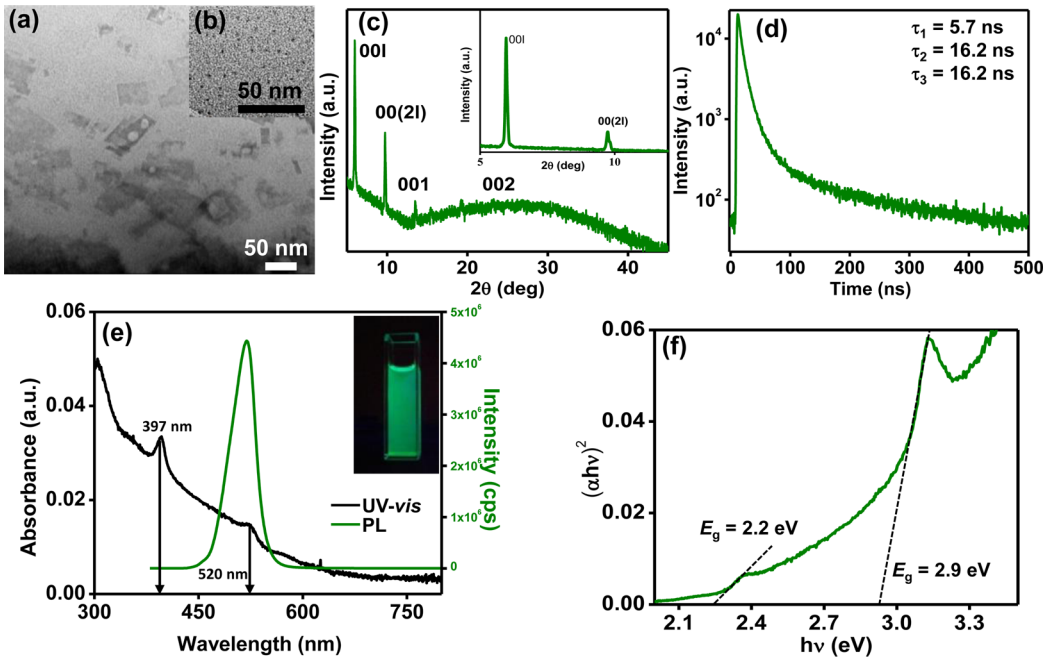

Figure 6. $MAPbBr_3$-based layered 2-D perovskite nanostructures: (a) and (b) TEM images, (c) XRD pattern, (d) PL lifetime decay (triexponential fit), (e) UV−vis and PL spectra (excitation wavelength 365 nm) (inset: photograph of the colloid), and (f) Tauc plot obtained from the UV−vis data.

DOI: 10.1021/acsami.5b10208
ACS Appl. Mater. Interfaces 2016, 8, 854−861

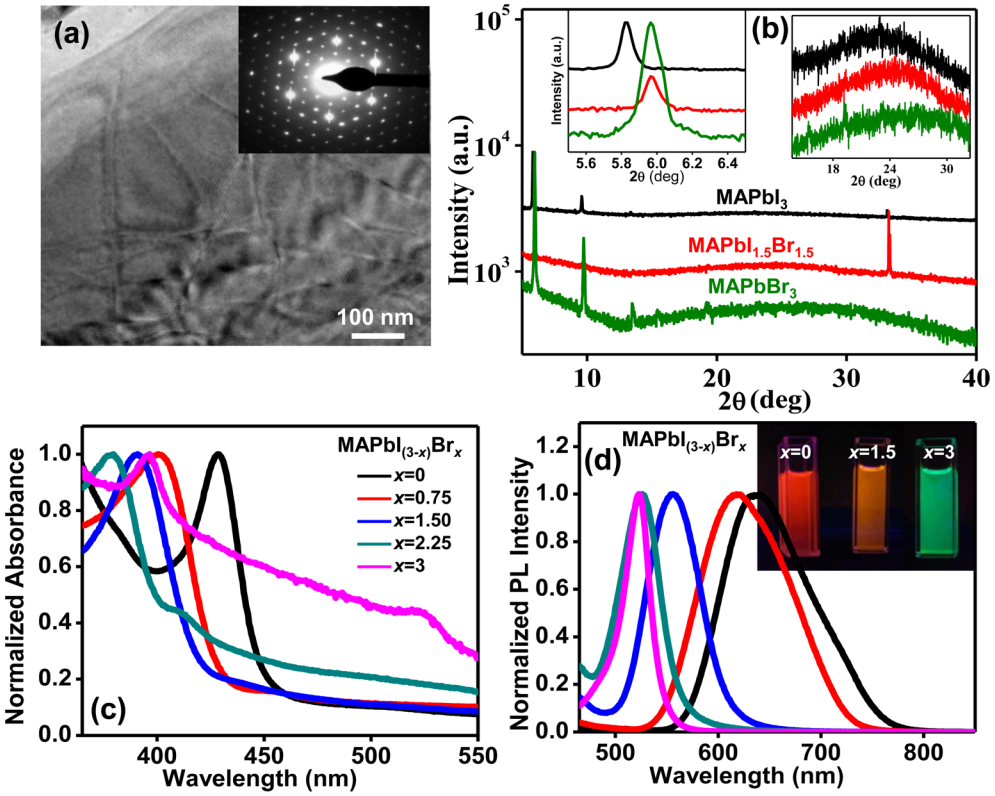

Figure 7. Mixed-halide $MAPbI_{1.5}Br_{1.5}$-based layered 2-D perovskite: (a) TEM image, (a, inset) SAEDP, and (b) XRD pattern. Layered 2-D perovskites: $MAPbI_3$, $MAPbI_{2.25}Br_{0.75}$, $MAPbI_{1.5}Br_{1.5}$, $MAPbI_{0.75}Br_{2.25}$, and $MAPbIBr_3$; (c) normalized UV−vis spectra, (d) normalized PL spectra (excitation wavelength 365 nm), and (d, inset) photographs of the colloids of indicted compositions.

confirms its single-crystal nature (Supporting Information Figure S4). Figure 7b shows the XRD pattern of this mixed-halide material, along with the XRD patterns from $MAPbI_3$ (Figure 3b) and $MAPbBr_3$ (Figure 6c). The inset in Figure 7b shows that the maximum in the broad hump for $MAPbI_{1.5}Br_{1.5}$ is between those for $MAPbI_3$ and $MAPbBr_3$, as expected. It is reported that for mixed-halide-based layered 2-D perovskite structures, Br^- preferentially occupies the apical positions in the Pb-X octahedra.[28] Because the ionic radius of Br^- is smaller than that of I^-,[36] the overall structure of $MAPbI_{1.5}Br_{1.5}$ is dominated by the Br-based layered 2-D perovskite. Also, this results in the smaller $d_{(00l)}$ and $d_{[00(2l)]}$ interlayer spacing of 14.8 and 9 Å, respectively, in $MAPbI_{1.5}Br_{1.5}$ based nanostructures compared to those in $MAPbI_3$-based nanostructures.

Figure 7c shows the normalized absorbance spectra for mixed-halide layered 2-D perovskites: $MAPbI_3$, $MAPbI_{2.25}Br_{0.75}$, $MAPbI_{1.5}Br_{1.5}$, $MAPbI_{0.75}Br_{2.25}$, and $MAPbBr_3$. Sharp excitonic features corresponding to single absorption peak are seen in each case, and the photographs of the colloids (Figure 7d, inset) show the corresponding colors. The normalized PL peaks (Figure 7d) are systematically blue-shifted with increasing Br content. Additionally, the PL line width is also seen to decrease considerably from full width at half-maximum (fwhm) from 102 nm down to 30 nm with increasing Br content. In the case of $MAPbBr_3$ perovskites the emission characteristics are mainly excitonic in nature, while in the case of $MAPbI_3$ perovskites they are mainly observed due to "self-trapped excitonic" character which results in the PL-peak broadening. Thus, in the mixed-halide-based perovskites, the increasing substitution of I^- by Br^- progressively reduces the self-trapping effect. Because the electronegativity of Br^- is higher than that of I^-, in the mixed halide cases, the Br atom substitution in lead iodide crystal framework affects the overall band structure allowing the effective band gap tuning over the broad visible range.

3.5. X-ray Photoelectron Spectroscopy (XPS) Studies.

The XPS data in Figure 8 provide further insights into the structural aspects of these as-formed hybrid nanomaterials. In the XPS data in Figure 8a for the three compositions, $MAPbI_3$, $MAPbI_{1.5}Br_{1.5}$, and $MAPbBr_3$, two symmetric peaks of Pb $4f_{7/2}$ and Pb $4f_{5/2}$ are observed at binding energy (BE) values of 138.2 and 143.0 eV, respectively. The energy difference due to spin−orbit splitting of 4f orbital is 4.8 eV, which is in agreement with the literature values.[37] No sign of metallic Pb was observed in these three compositions. The XPS data in Figure 8b show two peaks corresponding to I $3d_{5/2}$ and I $3d_{3/2}$ at BE values of 618.4 and 629.9 eV, respectively, with the spin−orbit splitting energy of 10.5 eV. The peak positions for $MAPbI_3$ and $MAPbI_{1.5}Br_{1.5}$ are almost overlapping.

The N_{1S} XPS data for all the three compositions are plotted in Figure 8c. For $MAPbI_3$, the N_{1S} data can be fitted to two peaks at 399.3 and 401.1 eV. The peak at 399.3 eV can be attributed to the presence of free amine ($-NH_2$) group of OA capping the 0-D QDs, while the peak at 401.1 eV can be attributed to NH_3^+ in MAI,[38] confirming the two types of nitrogen attached to the lead-halide framework. The NH_3^+ occupies the corner positions of perovskite unit cells and $-NH_2$ group intercalates and separates the inorganic lead iodide sheets. However, in the case of $MAPbI_{1.5}Br_{1.5}$, and $MAPbBr_3$ three peaks can be deconvoluted at 399.3, 400.4, and 401.3 eV, as shown in Figure 8c. Because Br-containing perovskite crystallizes into 2-D nanosheets as well, the additional 400.4 eV BE peak can be attributed to the $-NH_2$ group of the intercalated OA. In the $MAPbBr_3$ XPS data in Figure

DOI: 10.1021/acsami.5b10208
ACS Appl. Mater. Interfaces 2016, 8, 854−861

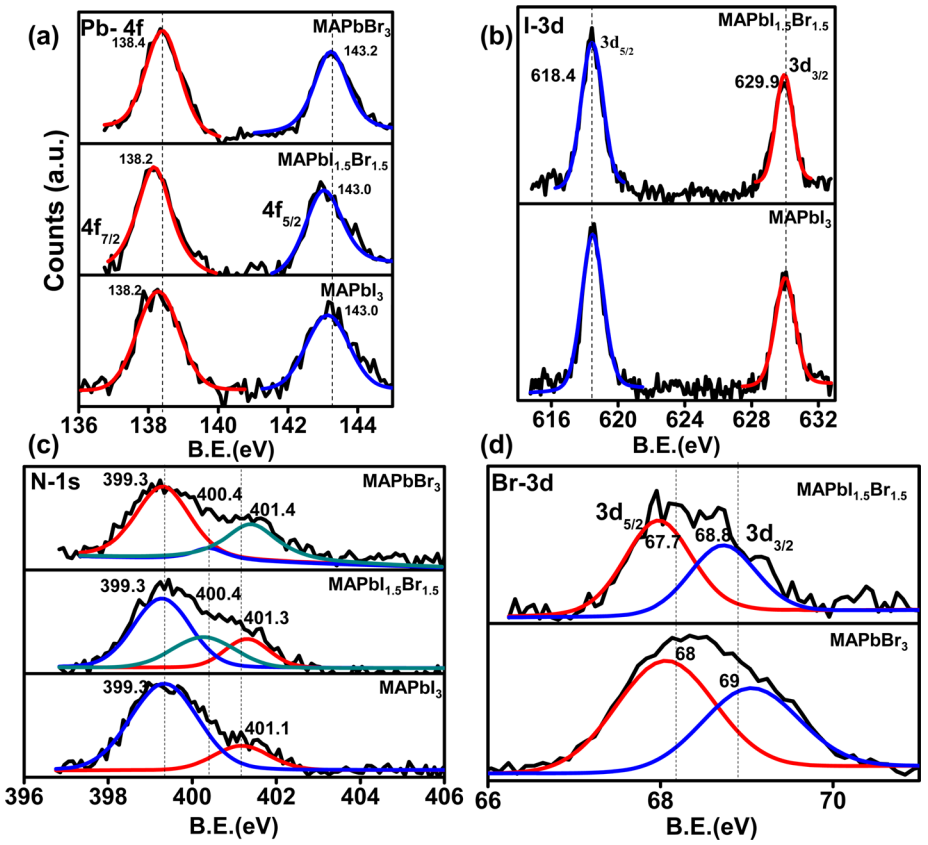

Figure 8. XPS data: (a) Pb-4f ($MAPbI_3$, $MAPbI_{1.5}Br_{1.5}$, $MAPbBr_3$), (b) I-3d ($MAPbI_3$, $MAPbI_{1.5}Br_{1.5}$), (c) N-1s ($MAPbI_3$, $MAPbI_{1.5}Br_{1.5}$, $MAPbBr_3$), and (d) Br-3d ($MAPbBr_3$, $MAPbI_{1.5}Br_{1.5}$).

8d the BE peak positions for Br $3d_{5/2}$ and Br $3d_{3/2}$ are at 68.0 and 69.0 eV, respectively, which are at somewhat higher BE compared to $MAPbI_{1.5}Br_{1.5}$. This can be attributed to the changes caused to the electron density distribution in the bond by the more electronegative Br.

4. SUMMARY

We have demonstrated the use of modified electrospray-assisted antisolvent−solvent extraction protocol for the synthesis of 0-D QDs and 2-D nanosheets of I- and Br-based, as well as mixed halide, hybrid perovskite systems. The 0-D QDs result via oleylamine (OA) capping, while the 2D nanosheets are realized via OA intercalation. The $MAPbI_3$ and $MAPbBr_3$ 0-D QDs show interesting optical properties, whereas the mixed-halide 2-D layered perovskite nanostructures show unusual luminescence properties. The optical band gaps and emission characteristics of these colloidal mixed-halide nanomaterials can be tuned over a broad range of visible spectral region via compositional tailoring.

■ ASSOCIATED CONTENT

Supporting Information

The Supporting Information is available free of charge on the ACS Publications website at DOI: 10.1021/acsami.5b10208.

FE-SEM images for OA variation; PL data for OA variation; AFM image and height profile for $MAPbI_3$ based layered perovskite; TEM images of $MAPbI_{1.5}Br_{1.5}$ based layered perovskite. (PDF)

■ AUTHOR INFORMATION

Corresponding Authors

*E-mail: rounakn@gmail.com.

*E-mail: satishogale@iiserpune.ac.in.

Author Contributions

All authors have given approval to the final version of the manuscript.

Notes

The authors declare no competing financial interest.

■ ACKNOWLEDGMENTS

R.N. and S.N. acknowledge the CSIR for senior research fellowship. R.N., S.N., G.S.N., and S.B.O. thank the APEX Phase II program (DST), (grant no. C.Dy.No. 2609/IFD/2015-16) TAPSUN (CSIR), and MNRE, Government of India for research funding. Y.Z. and N.P.P. acknowledge the National Science Foundation (grant no. DMR-1305913) for supporting the work at Brown University. We thank Dr. Sumati Patil and Prof. Aparna Deshpande (IISER, Pune) for help with the AFM measurements.

■ REFERENCES

(1) Green, M. A.; Ho-Baillie, A.; Snaith, H. The Emergence of Perovskite Solar Cell. *Nat. Photonics* **2014**, *8*, 506−514.

(2) Park, N. G. Organometal Perovskite Light Absorbers Towards a 20% Efficiency Low-Cost Solid State Mesoscopic Solar Cell. *J. Phys. Chem. Lett.* **2013**, *4*, 2423−2429.

(3) Kojima, A.; Teshima, K.; Shirai, Y.; Miyasaka, T. Organometal Lead Halide Perovskites as Visible Light Sensitizers for Photovoltaic Cells. *J. Am. Chem. Soc.* **2009**, *131*, 6050−6051.

DOI: 10.1021/acsami.5b10208
ACS Appl. Mater. Interfaces 2016, 8, 854−861

(4) Stranks, S. D.; Eperon, G.; Grancini, G.; Menelaou, C.; Alcocer, M. J. P.; Leijtens, T.; Herz, L. M.; Petrozza, A.; Snaith, H. J. Electron − Hole Diffusion Lengths Exceeding 1 Micrometer in an Organometal Trihalide Perovskite Absorbers. *Science* **2013**, *342*, 341−344.
(5) Xing, G.; Mathews, N.; Sun, S.; Lim, S. S.; Lam, Y. M.; Grätzel, M.; Mhaisalkar, S.; Sum, T. C. Long Range Balanced Electron and Hole Transport Lengths in Organic Inorganic $CH_3NH_3PbI_3$. *Science* **2013**, *342*, 344−347.
(6) Fu, Y.; Meng, F.; Rowley, M. B.; Thompson, B. J.; Shearer, M. J.; Ma, D.; Hamers, R. J.; Wright, J. C.; Jin, S. Solution Growth of Single Crystal Methylammonium Lead Halide Perovskite Nanostructures for Optoelectronic and Photovoltaic Applications. *J. Am. Chem. Soc.* **2015**, *137*, 5810−5818.
(7) Di, D.; Musselman, K. P.; Li, G.; Sadhanala, A.; Ievskaya, Y.; Song, Q.; Tan, Z. K.; Lai, M. L.; MacManus-Driscoll, J. L.; Greenham, N. C.; Friend, R. H. Size-Dependent Photon Emission from Organometal Halide Perovskite Nanocrystals Embedded in an Organic Matrix. *J. Phys. Chem. Lett.* **2015**, *6*, 446−450.
(8) Zhu, H.; Fu, Y.; Meng, F.; Wu, X.; Gong, Z.; Ding, Q.; Gustafsson, M. V.; Trinh, M. T.; Jin, S.; Zhu, X. Y. Lead Halide Perovskite Nanowire Lasers with Low Lasing Thresholds and High Quality Factors. *Nat. Mater.* **2015**, *14*, 636−642.
(9) Schmidt, L. C.; Pertegás, A.; González-Carrero, S.; Malinkiewicz, O.; Agouram, S.; Mínguez Espallargas, G.; Bolink, H. J.; Galian, R. E.; Pérez-Prieto, J. P. Nontemplate Synthesis of $CH_3NH_3PbBr_3$ Perovskite Nanoparticles. *J. Am. Chem. Soc.* **2014**, *136*, 850−853.
(10) Zhang, F.; Zhong, H.; Chen, C.; Wu, X. G.; Hu, X.; Huang, H.; Han, J.; Zou, B.; Dong, Y. Brightly Luminescent and Color Tunable Colloidal $CH_3NH_3PbX_3$ (X = Br, I, Cl) Quantum Dots: Potential Alternatives for Display Technologies. *ACS Nano* **2015**, *9*, 4533−4542.
(11) Kollek, T.; Gruber, D.; Gehring, J.; Zimmermann, E.; Schmidt-Mende, L.; Polarz, S. Porous and Shape Anisotropic Single Crystal of Semiconductor Perovskite $CH_3NH_3PbI_3$ from a Single Source Precursor. *Angew. Chem., Int. Ed.* **2015**, *54*, 1341−1346.
(12) Jeon, N. J.; Noh, J. H.; Kim, Y. C.; Yang, W. S.; Ryu, S.; Seok, S. Solvent Engineering for High-Performance Inorganic-Organic Hybrid Perovskite Solar Cells. *Nat. Mater.* **2014**, *13*, 897−903.
(13) Zhou, Y.; Yang, M.; Wu, W.; Vasiliev, A. L.; Zhu, K.; Padture, N. P. Room Temperature Crystallization of Hybrid- Perovskite Thin Films *via* Solvent-Solvent Extraction for High-Performance Solar Cells. *J. Mater. Chem. A* **2015**, *3*, 8178−8184.
(14) Kumar, P. S.; Sundaramurthy, J.; Sundarrajan, S.; Babu, V. J.; Singh, G.; Allakhverdiev, S. I.; Ramakrishna, S. Hierarchical Electrospun Nanofibers for Energy Harvesting, Production and Environmental Remediation. *Energy Environ. Sci.* **2014**, *7*, 3192−3222.
(15) Kumawat, N.; Dey, A.; Narasimhan, K. L.; Kabra, D. Near Infrared to Visible Electroluminescent Diodes based on Organometallic Halide Perovskites: Structural and Optical Investigation. *ACS Photonics* **2015**, *2*, 349−354.
(16) Eperon, G. E.; Stranks, S. D.; Menelaou, C.; Johnston, M. B.; Herz, L. M.; Snaith, H. J. Formamidinium Lead Trihalide: a Broadly Tunable Perovskite for Efficient Planar Heterojunction Solar Cells. *Energy Environ. Sci.* **2014**, *7*, 982−988.
(17) Burschka, J.; Pellet, N.; Moon, S. J.; Humphry-Baker, R.; Gao, P.; Nazeeruddin, M. K.; Grätzel, M. Sequential Deposition as a Route to High-Performance Perovskite-Sensitized Solar Cells. *Nature* **2013**, *499*, 316−319.
(18) Mourdikoudis, S.; Liz-Marzán, L. M. Oleylamine in Nanoparticle Synthesis. *Chem. Mater.* **2013**, *25*, 1465−1476.
(19) Tyagi, P.; Arveson, S. M.; Tisdale, W. A. Colloidal Organohalide Perovskite Nanoplatelets Exhibiting Quantum Confinement. *J. Phys. Chem. Lett.* **2015**, *6*, 1911−1916.
(20) Sichert, J. A.; Tong, Y.; Mutz, N.; Vollmer, M.; Fischer, M.; Milowska, K. Z.; García Cortadella, R.; Nickel, B.; Cardenas-Daw, C.; Stolarczyk, J. K.; Urban, A. S.; Feldmann, J. Quantum Size Effect in Organometal Halide Perovskite Nanoplatelets. *Nano Lett.* **2015**, *15*, 6521−6527.
(21) Dou, L.; Wong, A. B.; Yu, Y.; Lai, M.; Kornienko, N.; Eaton, S. W.; Fu, A.; Bischak, C. G.; Ma, J.; Ding, T.; Ginsberg, N. S.; Wang, L.-W.; Alivisatos, A.; Yang, P. Atomically Thin Two Dimensional Organic-Inorganic Hybrid Perovskite. *Science* **2015**, *349*, 1518−1521.
(22) Cheng, Z.; Lin, J. Layered Organic-Inorganic Hybrid Perovskites: Structure, Optical Properties, Film preparation, Patterning and Templating Engineering. *CrystEngComm* **2010**, *12*, 2646−2662.
(23) Zheng, Z.; Liu, A.; Wang, S.; Wang, Y.; Li, Z.; Lau, W. M.; Zhang, L. *In Situ* Growth of Epitaxial Lead Iodide Films Composed of Hexagonal Single Crystal. *J. Mater. Chem.* **2005**, *15*, 4555−4559.
(24) Venkataraman, N. V.; Bhagyalakshmi, S.; Vasudevan, S.; Seshadri, R. Conformation and Orientation of Alkyl Chains in the Layered Organic-Inorganic Hybrids: $(C_nH_{2n+1}NH_3)PbI_4$ (n = 12,16,18). *Phys. Chem. Chem. Phys.* **2002**, *4*, 4533−4538.
(25) Mitzi, D. B.; Feild, C. A.; Harrison, W. T. A.; Guloy, A. M. Conducting Tin Halides with a Layered Organic-Based Perovskite Structure. *Nature* **1994**, *369*, 467−469.
(26) Navas, J.; Sánchez-Coronilla, A.; Gallardo, J. J.; Cruz Hernandez, N.; Piñero, J. M.; Alcántara, R.; Fernández-Lorenzo, C.; De los Santos, D. M.; Aguilar, T.; Martín-Calleja, J. New Insights into Organic-Inorganic Hybrid Perovskite $CH_3NH_3PbI_3$ Nanoparticles: An Experimental and Theoretical Study of Doping of Pb^{2+} sites with Sn^{2+}, Sr^{2+}, Cd^{2+} and Ca^{2+}. *Nanoscale* **2015**, *7*, 6216−6229.
(27) Papagiannouli, I.; Maratou, E.; Koutselas, I.; Couris, S. Synthesis and Characterization of Nonlinear Optical Properties of Novel Hybrid Organic-Inorganic Semiconductor Lead Iodide Quantum Wells and Dots. *J. Phys. Chem. C* **2014**, *118*, 2766−2775.
(28) Ahmad, S.; Prakash, G. V. Two-Step Fabrication of R-$PbI_{4(1-y)}Br_{4y}$ Type Light Emitting Inorganic-Organic Hybrid Photonic Structure. *Opt. Mater. Express* **2014**, *4*, 101−110.
(29) Wu, X.; Trinh, M. T.; Zhu, X. Y. Excitonic Many Body Interactions in Two Dimensional Lead Iodide Perovskite Quantum Wells. *J. Phys. Chem. C* **2015**, *119*, 14714−14721.
(30) Ahmad, S.; Baumberg, J.; Vijaya Prakash, G. V. Structural Tunability and Switchable Exciton Emission in Inorganic-Organic Hybrids with Mixed Halides. *J. Appl. Phys.* **2013**, *114*, 233511−233513.
(31) Roldán-Carmona, C. R.; Gratia, P.; Zimmermann, I.; Grancini, G.; Gao, P.; Grätzel, M.; Nazeeruddin, M. K. High Efficiency Methylammonium Lead Triiodide Perovskite Solar Cells: the Relevance of Non-Stoichiometric Precursors. *Energy Environ. Sci.* **2015**, *8*, 3550−3556.
(32) Takeoka, Y.; Fukasawa, M.; Matsui, T.; Kikuchi, K.; Rikukawa, M.; Sanui, K. Intercalated Formation of Two-Dimensional and Multi Layered Perovskites in Organic Thin Films. *Chem. Commun.* **2005**, 378−380.
(33) Tanaka, K.; Takahashi, T.; Ban, T.; Kondo, T.; Uchida, K.; Miura, N. Comparative Study on the Excitons in Lead-Halide based Perovskite Type Crystals $CH_3NH_3PbBr_3$ $CH_3NH_3PbI_3$. *Solid State Commun.* **2003**, *127*, 619−623.
(34) Song, J.; Li, J.; Li, X.; Xu, L.; Dong, Y.; Zeng, H. Quantum Dot Light-Emitting Diodes Based on Inorganic Perovskite Cesium Lead Halides ($CsPbX_3$). *Adv. Mater.* **2015**, *27*, 7162−7167.
(35) Wang, Y.; Li, X.; Song, J.; Xiao, L.; Zeng, H.; Sun, H. All-Inorganic Colloidal Perovskite Quantum Dots: A New Class of Lasing Materials with Favorable Characteristics. *Adv. Mater.* **2015**, *27*, 7101−7108.
(36) Aharon, S.; Cohen, B. E.; Etgar, L. Hybrid Lead Halide Iodide and Lead Halide Bromide in Efficient Hole Conductor free Perovskite Solar Cells. *J. Phys. Chem. C* **2014**, *118*, 17160−17165.
(37) Morgan, W. E.; Van Wazer, J. R. Binding Energy Shifts in the X-ray Photoelectron Spectra of a Series of Related group IVA Compounds. *J. Phys. Chem.* **1973**, *77*, 964−969.
(38) Chen, S.; Goh, T. W.; Sabba, D.; Chua, J.; Mathews, N.; Huan, C. H. A.; Sum, T. C. Energy Level Alignment at the Methylammonium Lead Iodide/Copper Phthalocyanine Interface. *APL Mater.* **2014**, *2*, 081512−081517.

DOI: 10.1021/acsami.5b10208
ACS Appl. Mater. Interfaces 2016, 8, 854−861